Research Article | Vol. 28, No. 20 / 28 September 2020 / Optics Express 29895
Optics EXPRESS

Electrically generated optical waveguide in a lithium-niobate thin film

QINGMING CHEN,[1,2,3] YUJIAO ZHU,[1] DI WU,[4] TENGHAO LI,[1] ZHAOHUI LI,[5] CHAO LU,[2] KIN SENG CHIANG,[3] AND XUMING ZHANG[1,*]

[1]Department of Applied Physics, The Hong Kong Polytechnic University, Hong Kong SAR, China
[2]Department of Electronic and Information Engineering, The Hong Kong Polytechnic University, Hong Kong SAR, China
[3]Department of Electrical Engineering, City University of Hong Kong, 83 Tat Chee Ave., Kowloon, Hong Kong SAR, China
[4]School of Physics and Microelectronics, Zhengzhou University, Zhengzhou, Henan 450052, China
[5]School of Electronics and Information Engineering, State Key Laboratory of Optoelectronic Materials and Technologies, Sun Yat-sen University, Guangzhou 510275, China
*apzhang@polyu.edu.hk

Abstract: This paper reports an electrically generated optical waveguide for the transverse-magnetic wave. The waveguide is formed in a z-cut single-crystal lithium-niobate (LN) thin film by the electro-optic effect, where the extraordinary refractive index (RI) of the LN film is increased by a voltage applied to patterned electrodes that define the waveguide geometry. Such a waveguide can be made to exist or disappear by turning on or off the applied voltage. A straight waveguide and an S-bend waveguide with an RI contrast of ~0.004 are generated at a voltage of 200 V. The propagation loss of the generated waveguide measured at the wavelength 532 nm is 1.8 dB/cm. Electrically generated optical waveguides could fulfill useful functions in photonic integrated circuits, such as reconfigurable cross connect and switching that require wavelength-independent and mode-independent operation.

1. Introduction

Optical waveguides are the basic structures in semiconductor lasers, optical devices, and optical interconnect. Many material systems have been developed for forming waveguide devices, such as gallium arsenide [1], indium phosphide [2], silicon/silica [3,4], and lithium niobate (LN) [5]. Among these, LN possesses several distinct advantages, which include a strong acousto-optic effect [6,7], a broad transparent window (0.4–5 μm) [8], and a high electro-optic (EO) coefficient (r_{33} = 32.2 pm/V at 633 nm for bulk LN) [9,10]. LN has been widely used for forming waveguide devices, such as parametric light sources [11], switches [12], modulators [13], frequency comb generators [14,15], etc. Recently, wafer-scale single-crystal LN thin film on SiO_2 cladding, namely LN on insulator (LNOI), has become commercially available [16]. The large refractive-index (RI) contrast ($\Delta n \approx 0.7$) between LN and SiO_2 allows light to be confined in a submicron-thick LN film. The small mode size (~1 μm^2) and the low loss (0.3 dB/cm) [17] available with LNOI make it an excellent platform for building dense photonic integrated circuits (PICs) [8]. The high EO coefficient of bulk LN is also preserved in an LN thin film (r_{33} = 29.5 pm/V) [18]. Taking all these advantages of thin-film LN, several ultrafast EO modulators based on LNOI have been demonstrated recently, which include, for example, a monolithically integrated CMOS-compatible 45 GHz modulator with a half-wave voltage of 1.4 V [19] and a hybrid silicon/LN 70 GHz modulator with a half-wave voltage of 2.2 V [20].

A number of methods are available for the fabrication of optical waveguides on the LNOI platform, such as proton exchange [21,22], strip loading [23,24], wet/dry etching [17,25], and

#405029 https://doi.org/10.1364/OE.405029
Journal © 2020 Received 10 Aug 2020; revised 12 Sep 2020; accepted 14 Sep 2020; published 21 Sep 2020

Optics EXPRESS

ion milling [26,27]. These methods are developed for the production of permanent waveguides. In this paper, we propose a method of forming an LNOI waveguide whose existence depends on an applied voltage. Our method is based on depositing patterned electrodes on a z-cut LN film. When a voltage is applied to the electrodes, the EO effect of the LN film increases its extraordinary RI and thus generates a waveguide with dimensions defined by the electrodes. Such a "waveguide on demand" could find applications where wavelength-independent reconfigurable light paths are required. To demonstrate the idea, we fabricate a straight waveguide and an S-bend waveguide with the proposed method and characterize them at the wavelength 532 nm. The waveguides have a cross-sectional area of 4.5×0.7 μm^2 and an RI contrast of ~0.004, which are generated with a voltage of 200 V. The propagation loss of the generated waveguide is 1.8 dB/cm.

2. Principle and analysis

Figure 1(a) shows the structure of a z-cut LN film that has an ordinary RI of $n_o = 2.2777$ and an extraordinary RI of $n_e = 2.2102$, which is sandwiched between two SiO_2 cladding layers that have an RI of $n_{SiO2} = 1.46$. The thickness of the LN film is 700 nm and that of each cladding is 500 nm. A 100 nm gold (Au) film is buried between the lower cladding and the LN substrate as a ground electrode, while an indium tin oxide (ITO) film with a finite width is deposited on the upper cladding to form a top electrode. When a (positive) voltage is applied across the top electrode and the ground electrode, an electric field is produced in the SiO_2 and LN layers, which results in an increase in the extraordinary RI of the LN film in the region below the top electrode through the EO effect. This region can thus act as a waveguide core to provide light confinement in the LN film, as shown in Fig. 1(b). The width of the generated core is determined by the width of the top electrode and the direction of the waveguide along the LN film depends on the layout of the top electrode. Figures 1(c) and 1(d) show the layouts of the ITO electrodes for the generation of a straight waveguide and an S-bend waveguide, respectively.

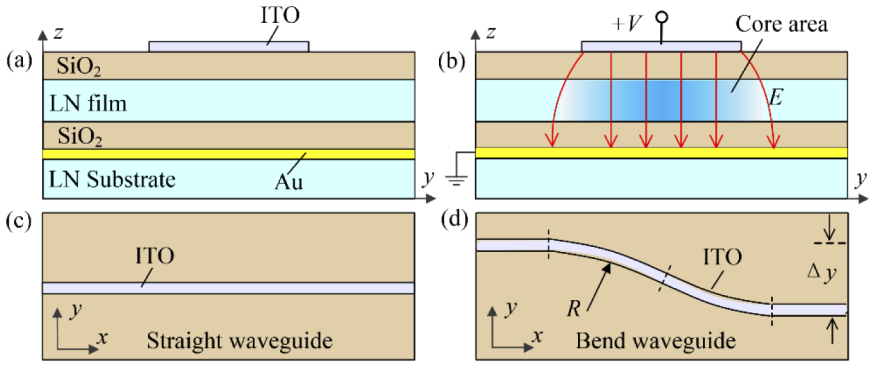

Fig. 1. Schematic diagrams showing (a) the structure of a z-cut LN thin film sandwiched between two SiO_2 cladding layers that incorporates a buried Au ground electrode and an ITO top electrode; (b) the waveguide core generated in the LN film by the electric field E with an applied voltage V; and the layouts of the ITO electrodes for the generation of (c) a straight waveguide and (d) an S-bend waveguide with a bend radius R and a lateral offset Δy between the input and output ends.

For an electric field produced in the y-z plane, as shown in Fig. 1(b), the changes in the ordinary RI and the extraordinary RI of the LN film, denoted as Δn_o and Δn_e, respectively, are given by [10]

$$\Delta n_o(E) = -\frac{1}{2} n_o^3 \left(r_{22} E_y + r_{13} E_z\right) \tag{1}$$

Optics EXPRESS

$$\Delta n_e(E) = -\frac{1}{2} n_e^3 r_{33} E_z \tag{2}$$

where E_y and E_z are the electric field components along the y and z directions, respectively, and $r_{22} = 6.7$ pm/V, $r_{13} = 10$ pm/V, and $r_{33} = 29.5$ pm/V are the EO coefficients. For the electrode configuration shown in Fig. 1(b), E_z is the dominant component and has a negative value.

At a given applied voltage, we can calculate the electric field distributions produced in the LN film and then the RI profiles from the above equations by the finite element method (COMSOL). The results for an applied voltage of 200 V are shown in Fig. 2(a) and Fig. 2(b) for Δn_o and Δn_e, respectively. In the region below the top electrode, the electric field consists of mainly the z-component; the y-component is significant only near the edges of the top electrode. Because the y-component has an antisymmetric distribution, the change in the ordinary RI, Δn_o, has an asymmetric distribution in the y direction, which has a peak value of about +0.002 on one side and a smallest value of about –0.001 on the other side, as shown in Fig. 2(a). Therefore, the generated RI profile is not suitable for the guidance of the transverse electric (TE) wave, which is governed by the ordinary RI. On the other hand, the change in the extraordinary RI, Δn_e, has a step-like symmetric distribution with a peak value of about +0.004, as shown in Fig. 2(b), which is suitable for the guidance of the transverse magnetic (TM) wave. The width of the top electrode is set to be 4.5 μm. The field distribution of the fundamental TM mode in the generated waveguide, calculated at the wavelength 532 nm with the finite element method, is shown in Fig. 2(c). Excellent mode confinement is obtained. Because the EO-induced RI increase is small, the width of the mode field in our waveguide, as shown in Fig. 2(c), is in general larger than that in a conventional etched LNOI waveguide. To achieve low-loss connection between our waveguide and an etched LNOI waveguide on the same chip, we could use a taper structure where the width of the etched waveguide is gradually increased towards the EO-induced waveguide to provide mode matching.

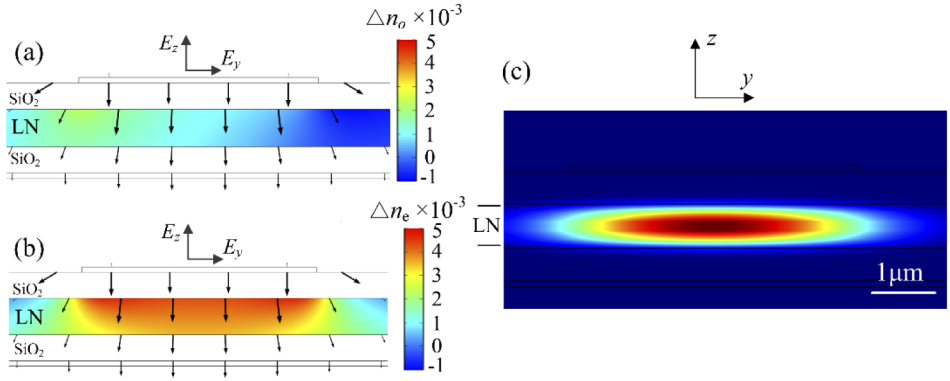

Fig. 2. Electric field distribution and the changes in (a) the ordinary RI and (b) the extraordinary RI, calculated at an applied voltage of 200 V, and (c) the field distribution of the fundamental TM mode supported by the RI profile in (b), calculated at the wavelength 532 nm.

Though we plan our experiments for the visible wavelength 532 nm, it is possible to apply the same method to the generation of waveguides for the near infrared regime. As the EO effect in the near infrared regime is weaker, a higher voltage for waveguide generation is required. According to our simulation, to increase the RI by 0.004 for single-mode operation at 1550 nm with a 6-μm wide top electrode, the voltage required is 219 V.

Optics EXPRESS

3. Experimental results and discussion

3.1. Fabrication process

The LNIO wafers used in our experiments came with the Au electrode (NANOLN) and it was only necessary for us to form the top SiO_2 layer and the ITO electrode. Figure 3 shows the main steps in the fabrication of the ITO-coated LNOI structure. A 500 nm SiO_2 layer was first deposited on the surface of a wafer by plasma enhanced chemical vapor deposition (PEVCD), which led to the structure shown in Fig. 3(a). A thin film of AZ5214 photoresist was then patterned on the sample as a mask, as shown in Fig. 3(b). A 100 nm ITO thin film was next deposited on the sample at room temperature by DC magnetic sputtering and the sample was subsequently immersed in acetone for 12 hours to remove the ITO-coated photoresist. This lift-off method resulted in an ITO strip on the surface of the sample, as shown in Fig. 3(c). The sample was finally annealed at 300 °C for 3 hours to reduce the resistance of the ITO electrode. A microscopic image of the sample with the ITO electrode is shown in Fig. 3(d). Two kinds of samples were prepared: one contained a straight ITO electrode and the other contained an S-bend ITO electrode.

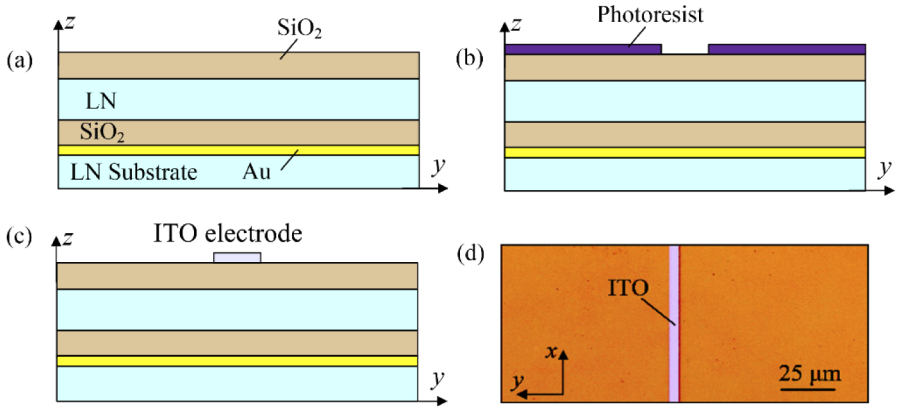

Fig. 3. Main fabrication steps: (a) deposition of a SiO_2 layer on the surface of a wafer, (b) patterning of a photoresist film deposited on the sample, and (c) formation of an ITO electrode by the lift-off method. (d) Microscopic image of an ITO-deposited sample (top view).

3.2. Characterization of the EO effect

To characterize the EO effect, we directly deposited a 50 nm ITO film on a LNOI wafer (the sample contained no upper SiO_2 cladding). The RIs of the LN film were measured at the wavelength 632.8 nm with a commercial prism-coupler system (Model 2010, Metricon), where the use of a TE-polarized beam gave the ordinary RI and the use of a TM-polarized beam gave the extraordinary RI. The ordinary and extraordinary RIs of the LN film measured at different applied voltages are shown in Fig. 4(a) and Fig. 4(b), respectively. The RIs increase linearly with the applied voltage. As the applied voltage increases from 0 V to 150 V, the ordinary and extraordinary RIs increase by 0.0013 and 0.0047, respectively. The results calculated from Eq. (1) and Eq. (2) are also shown in Fig. 4 for comparison. The calculated ordinary RIs are significantly larger than the measured values, which could be explained by the use of the EO coefficients (r_{22} and r_{13}) of bulk LN in the calculation of the ordinary RI, as the EO coefficients of the LN film are expected to be smaller [18]. On the other hand, the agreement for the extraordinary RI is much better, as the r_{33} value used in the calculation is for an LN film. In addition, the presence

Optics EXPRESS

of the ITO electrode, which is ignored in the calculation of the RIs by the prism-coupler system, affects the accuracy of the measured values.

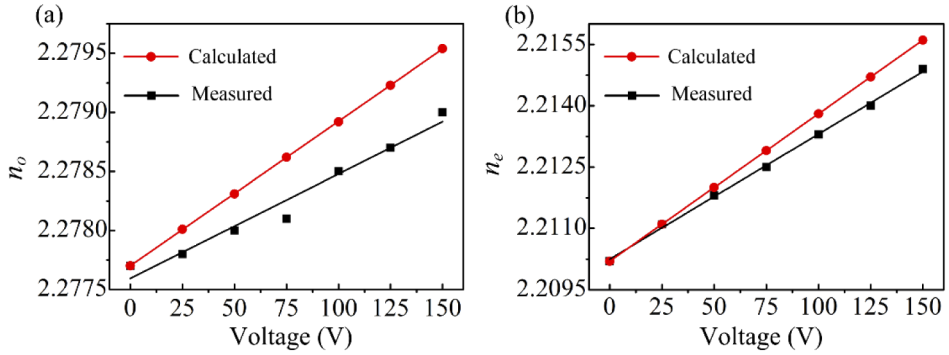

Fig. 4. (a) Ordinary and (b) extraordinary RIs of an LN film measured at different applied voltages with an ITO-coated LN sample (Measured), together with the results calculated from Eq. (1) and Eq. (2) (Calculated).

3.3. *Characterization of electrically generated waveguides*

To characterize the electrically generated waveguide, we applied a voltage to the electrodes of a sample under test with a voltage amplifier (Trek Model 2210) and launched a green laser beam at 532 nm into the generated waveguide with a lensed fiber. A polarization controller was placed along the fiber lead to ensure that the beam launched into the sample was TM-polarized. Two sets of charge-coupled device (CCD) imaging systems were used, with the vertical one for alignment and top view observation and the horizontal one for the detection of the output light from the sample. The output power could be measured by replacing the horizontal CCD camera with a photodetector. The experimental setup is shown schematically in Fig. 5.

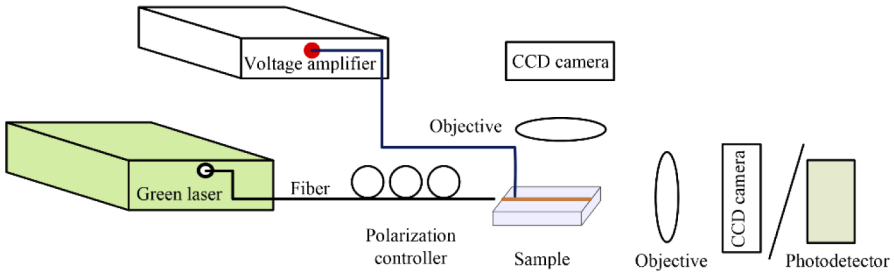

Fig. 5. Experimental setup for waveguide characterization.

The close agreement between the theory and the measurement shown in Fig. 4(b) indicates that our estimation of the EO-induced RI change is accurate. According to our numerical results shown in Fig. 2(b), an applied voltage of 200 V can increase the extraordinary RI by ~0.004, which is sufficient to provide strong guidance for the TM wave, as shown in Fig. 2(c). In our experiments, we used an applied voltage of 200 V for waveguide generation.

Figure 6 shows some photos taken from the CCD cameras. For a sample that contained a straight 10-mm long electrode, when no voltage was applied, no light could be seen at the output end, as shown in Fig. 6(a). When a voltage of 200 V was applied, a bright light spot appeared at the output end, as shown by the side view in Fig. 6(b) and the top view in Fig. 6(c), which confirms successful generation of a waveguide. The inset in Fig. 6(b) is a near-field image of

Optics EXPRESS

the output light, which shows a flat mode pattern as predicted in Fig. 2(c). The power of the laser beam from the lensed fiber was 11.0 dBm and the output power from the waveguide was 2.5 dBm. By comparing the output power from another sample that had a straight 5-mm long electrode driven at the same voltage, we found that the waveguide loss was ~1.8 dB/cm and the fiber/waveguide coupling loss was ~6.7 dB. For the photos shown in Figs. 6(a) and 6(b), an aperture was used to block the background light from the LN film.

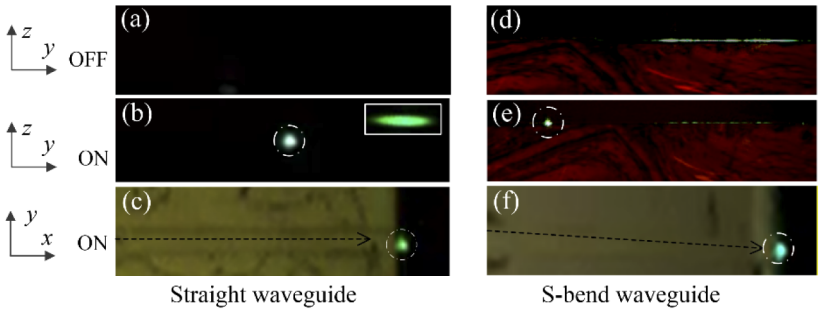

Fig. 6. Photos taken from the CCD cameras to experimentally demonstrate the operation of electrically generated waveguides. The sample with a 10-mm long straight electrode shows (a) no output light in the absence of the applied voltage and strong confined output light in the presence of the applied voltage, as seen from (b) the output end and (c) the top of the sample, where the inset in (b) shows a near-field image of the output light. The sample with an S-bend electrode shows (d) unconfined output light across the LN film in the absence of the applied voltage and strong confined output light in the presence of the applied voltage, as seen from (e) the output end and (f) the top of the sample. For the photos shown in (a) and (b), an aperture was used to block the background light.

We repeated the same measurements for a sample that contained an S-bend electrode with $R = 5$ mm and $\Delta y = 0.46$ mm. The sample was 5 mm long, which consisted of two 1-mm long straight sections at the two ends and a 3-mm long bent section in the middle, as shown schematically in Fig. 1(d). When no voltage was applied to the electrodes, the input light was seen to spread over the entire LN film, as shown in Fig. 6(d), which indicates no light confinement in the y direction. When a voltage of 200 V was applied to the electrodes, a bright light spot was observed, as shown by the side view in Fig. 6(e) and the top view in Fig. 6(f), which confirms successful generation of an S-bend waveguide. By comparing the power measurements for the straight waveguide and the bend waveguide, we found that the waveguide bend introduced an additional loss of ~0.18 dB.

Our electrically generated waveguides are stable. We do not observe significant long-term drifts in their transmission characteristics. We should also note that waveguides can be generated at lower voltages with some penalties in the propagation loss, and such waveguides suffer from larger bend losses because of their weaker mode confinement. On the other hand, it is possible to reduce the bend loss by using a waveguide generated at a higher voltage, though it would be difficult to achieve a bend radius smaller than 1 mm without introducing a significant bend loss.

3.4. Response time

We made an attempt to measure the response time of the waveguide generation process by applying a 5-kHz square-wave voltage (200 V) to the sample that contained a 10-mm long straight electrode. The output light from the generated waveguide was measured with a photodetector and the waveforms were displayed by an oscilloscope. The results are shown in Fig. 7, where A, B, and C label the signals from the function generator, the voltage amplifier, and the photodetector, respectively. A comparison of the signals A and B shows that the response time of the electrical

Optics EXPRESS

system is about 6.0 μs and the response time measured from the signal C is practically the same. Therefore, the response time in our measurement is limited by the electrical system rather than the intrinsic speed of the EO effect in an LN film, which is as fast as a few nanoseconds [28]. The use of a relatively high voltage to generate the waveguide makes it difficult to achieve a high switching speed (limited by the electrical system). One way to lower the driving voltage is to replace the ITO electrode with a graphene electrode, so that the upper SiO_2 cladding can be removed [29,30].

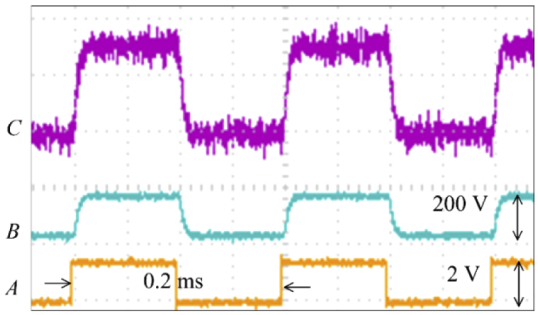

Fig. 7. Switching response of the electrically generated waveguide measured with the sample that contained a 10-mm long straight electrode, where A, B, and C label the signals from the function generator, the voltage amplifier, and the photodetector.

4. Conclusion

We have presented electrically generated optical waveguides on the LNOI platform based on the strong EO effect of the LN film, where the waveguide geometry and the propagation direction can be controlled by the width and the layout of the top electrode. By using a voltage of 200 V, we have successfully formed channel waveguides with an index contrast of ~0.004 to provide strong guidance for the TM wave. The propagation loss of our waveguides is ~1.8 dB/cm, measured at the wavelength 532 nm. It is possible to generate similar waveguides for operation in the near infrared regime by using somewhat higher voltages. The process of forming such waveguides is simple, as it involves no more than electrode deposition. It could be possible to lower the driving voltage by optimizing the electrode design. The ability to control the existence or disappearance of a waveguide electrically may offer new, special application possibilities, as such a switching operation, unlike those offered by conventional waveguide switches, is wavelength-independent and mode-independent.

Funding

City University of Hong Kong (9610452); Hong Kong Polytechnic University (1-ZE14, 1-ZE27, 1-ZVGH); Research Grants Council, University Grants Committee (152126/18E, 152127/17E, 152184/15E, 152219/19E).

Acknowledgments

The technical assistance and facility support from the Materials Research Centre (MRC) and the University Research Facility in Material Characterization and Device Fabrication (UMF) of The Hong Kong Polytechnic University are acknowledged.

Disclosures

The authors declare no conflicts of interest.

Optics EXPRESS

References

1. J. Wang, A. Santamato, P. Jiang, D. Bonneau, E. Engin, J. W. Silverstone, M. Lermer, J. Beetz, M. Kamp, and S. Höfling, "Gallium arsenide (GaAs) quantum photonic waveguide circuits," Opt. Commun. **327**, 49–55 (2014).
2. S. Arafin and L. A. Coldren, "Advanced InP Photonic Integrated Circuits for Communication and Sensing," IEEE J. Sel. Top. Quantum Electron. **24**(1), 1–12 (2018).
3. M. Ferrera, L. Razzari, D. Duchesne, R. Morandotti, Z. Yang, M. Liscidini, J. Sipe, S. Chu, B. Little, and D. Moss, "Low-power continuous-wave nonlinear optics in doped silica glass integrated waveguide structures," Nat. Photonics **2**(12), 737–740 (2008).
4. K. Wang, A. Nirmalathas, C. Lim, E. Wong, K. Alameh, H. Li, and E. Skafidas, "High-speed indoor optical wireless communication system employing a silicon integrated photonic circuit," Opt. Lett. **43**(13), 3132–3135 (2018).
5. W. Sohler, H. Hu, R. Ricken, V. Quiring, C. Vannahme, H. Herrmann, D. Büchter, S. Reza, W. Grundkötter, and S. Orlov, "Integrated optical devices in lithium niobate," Opt. Photonics News **19**(1), 24–31 (2008).
6. L. Shao, M. Yu, S. Maity, N. Sinclair, L. Zheng, C. Chia, A. Shams-Ansari, C. Wang, M. Zhang, and K. Lai, "Microwave-to-optical conversion using lithium niobate thin-film acoustic resonators," Optica **6**(12), 1498–1505 (2019).
7. Z. Yu and X. Sun, "Acousto-optic modulation of photonic bound state in the continuum," Light: Sci. Appl. **9**(1), 1–9 (2020).
8. Y. Qi and Y. Li, "Integrated lithium niobate photonics," Nanophotonics 1(ahead-of-print) (2020).
9. L. Arizmendi, "Photonic applications of lithium niobate crystals," Phys. Status Solidi A **201**(2), 253–283 (2004).
10. R. Weis and T. Gaylord, "Lithium niobate: summary of physical properties and crystal structure," Appl. Phys. A **37**(4), 191–203 (1985).
11. G. Fujii, N. Namekata, M. Motoya, S. Kurimura, and S. Inoue, "Bright narrowband source of photon pairs at optical telecommunication wavelengths using a type-II periodically poled lithium niobate waveguide," Opt. Express **15**(20), 12769–12776 (2007).
12. W. Jin and K. S. Chiang, "Mode switch based on electro-optic long-period waveguide grating in lithium niobate," Opt. Lett. **40**(2), 237–240 (2015).
13. E. L. Wooten, K. M. Kissa, A. Yi-Yan, E. J. Murphy, D. A. Lafaw, P. F. Hallemeier, D. Maack, D. V. Attanasio, D. J. Fritz, and G. J. McBrien, "A review of lithium niobate modulators for fiber-optic communications systems," IEEE J. Sel. Top. Quantum Electron. **6**(1), 69–82 (2000).
14. C. Wang, M. Zhang, M. Yu, R. Zhu, H. Hu, and M. Loncar, "Monolithic lithium niobate photonic circuits for Kerr frequency comb generation and modulation," Nat. Commun. **10**(1), 978 (2019).
15. M. Zhang, B. Buscaino, C. Wang, A. Shams-Ansari, C. Reimer, R. Zhu, J. M. Kahn, and M. Lončar, "Broadband electro-optic frequency comb generation in a lithium niobate microring resonator," Nature **568**(7752), 373–377 (2019).
16. G. Poberaj, H. Hu, W. Sohler, and P. Guenter, "Lithium niobate on insulator (LNOI) for micro-photonic devices," Laser Photonics Rev. **6**(4), 488–503 (2012).
17. H. Hu, R. Ricken, W. Sohler, and R. Wehrspohn, "Lithium niobate ridge waveguides fabricated by wet etching," IEEE Photonics Technol. Lett. **19**(6), 417–419 (2007).
18. L. Cai, Y. Kang, and H. Hu, "Electric-optical property of the proton exchanged phase modulator in single-crystal lithium niobate thin film," Opt. Express **24**(5), 4640–4647 (2016).
19. C. Wang, M. Zhang, X. Chen, M. Bertrand, A. Shams-Ansari, S. Chandrasekhar, P. Winzer, and M. Lončar, "Integrated lithium niobate electro-optic modulators operating at CMOS-compatible voltages," Nature **562**(7725), 101–104 (2018).
20. M. He, M. Xu, Y. Ren, J. Jian, Z. Ruan, Y. Xu, S. Gao, S. Sun, X. Wen, L. Zhou, L. Liu, C. Guo, H. Chen, S. Yu, L. Liu, and X. Cai, "High-performance hybrid silicon and lithium niobate Mach–Zehnder modulators for 100 Gbit s−1 and beyond," Nat. Photonics **13**(5), 359–364 (2019).
21. L. Cai, S. L. H. Han, and H. Hu, "Waveguides in single-crystal lithium niobate thin film by proton exchange," Opt. Express **23**(2), 1240–1248 (2015).
22. X. P. Li, K. X. Chen, and Z. F. Hu, "Low-loss bent channel waveguides in lithium niobate thin film by proton exchange and dry etching," Opt. Mater. Express **8**(5), 1322–1327 (2018).
23. S. Li, L. Cai, Y. Wang, Y. Jiang, and H. Hu, "Waveguides consisting of single-crystal lithium niobate thin film and oxidized titanium stripe," Opt. Express **23**(19), 24212–24219 (2015).
24. Y. Wang, Z. Chen, L. Cai, Y. Jiang, H. Zhu, and H. Hu, "Amorphous silicon-lithium niobate thin film strip-loaded waveguides," Opt. Mater. Express **7**(11), 4018–4028 (2017).
25. G. Ulliac, V. Calero, A. Ndao, F. Baida, and M.-P. Bernal, "Argon plasma inductively coupled plasma reactive ion etching study for smooth sidewall thin film lithium niobate waveguide application," Opt. Mater. **53**, 1–5 (2016).
26. S. Y. Siew, E. J. H. Cheung, H. Liang, A. Bettiol, N. Toyoda, B. Alshehri, E. Dogheche, and A. J. Danner, "Ultra-low loss ridge waveguides on lithium niobate via argon ion milling and gas clustered ion beam smoothening," Opt. Express **26**(4), 4421–4430 (2018).
27. M. F. Volk, S. Suntsov, C. E. Rüter, and D. Kip, "Low loss ridge waveguides in lithium niobate thin films by optical grade diamond blade dicing," Opt. Express **24**(2), 1386–1391 (2016).
28. L. Chen, Q. Xu, M. G. Wood, and R. M. Reano, "Hybrid silicon and lithium niobate electro-optical ring modulator," Optica **1**(2), 112–118 (2014).

Optics EXPRESS

29. Z. Chang, W. Jin, and K. S. Chiang, "Graphene electrodes for lithium-niobate electro-optic devices," Opt. Lett. **43**(8), 1718–1721 (2018).
30. W. Jin and K. S. Chiang, "Reconfigurable Three-Mode Converter Based On Cascaded Electro-Optic Long-Period Gratings," IEEE J. Sel. Top. Quantum Electron. **26**(5), 1–6 (2020).